Chemosphere 242 (2020) 125143

Contents lists available at ScienceDirect

Chemosphere

journal homepage: www.elsevier.com/locate/chemosphere

Ochratoxin A triggered intracerebral hemorrhage in embryonic zebrafish: Involvement of microRNA-731 and prolactin receptor

Ting-Shuan Wu [a], Yu-Ting Lin [a], Ying-Tzu Huang [a], Feng-Yih Yu [b, c, **], Biing-Hui Liu [a, *]

[a] Graduate Institute of Toxicology, College of Medicine, National Taiwan University, Taipei, Taiwan
[b] Department of Biomedical Sciences, Chung Shan Medical University, Taiwan
[c] Department of Medical Research, Chung Shan Medical University Hospital, Taichung, Taiwan

HIGHLIGHTS

- OTA induced intracerebral hemorrhage (ICH) in embryonic zebrafish.
- OTA interfered with the development of cerebral vasculature.
- The formation of central arteries (CtAs) was adversely affected by OTA.
- The miR-731/PRLRa axis involved in OTA-induced vascular defects and led to ICH.

GRAPHICAL ABSTRACT

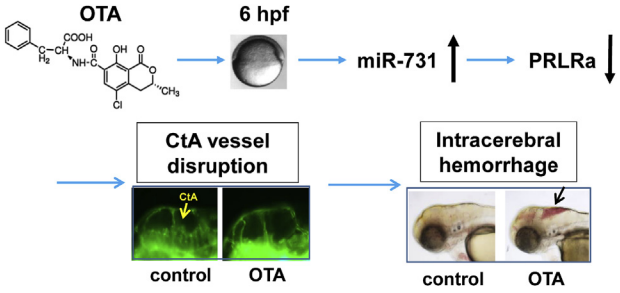

ARTICLE INFO

Article history:
Received 28 July 2019
Received in revised form
15 October 2019
Accepted 16 October 2019
Available online 21 October 2019

Handling Editor: David Volz

Keywords:
Ochratoxin A
Intracerebral hemorrhage
Vascular defect
microRNA-731
Prolactin receptor a
Zebrafish embryos

ABSTRACT

Ochratoxin A (OTA), a mycotoxin widely found in foodstuffs, reportedly damages multiple brain regions in developing rodents, but the corresponding mechanisms have not been elucidated. In this study, zebrafish embryos at 6 h post fertilization (hpf) were exposed to various concentrations of OTA and the phenomenon associated with intracerebral hemorrhage was observed at 72 hpf. Exposure of embryos to OTA significantly increased their hemorrhagic rate in a dose-dependent manner. Large numbers of extravagated erythrocytes were observed in the midbrain/hindbrain areas of Tg(fli-1a:EGFP; gata1:DsRed) embryos following exposure to OTA. OTA also disrupted the vascular patterning, especially the arch-shaped central arteries (CtAs), in treated embryos. Histological analysis revealed a cavity-like pattern in their hindbrain ventricles, implying the possibility of cerebral edema. OTA-induced intracerebral hemorrhage and CtA vessel defects were partially reversed by the presence of miR-731 antagomir or the overexpression of prolactin receptor a (*prlra*); *prlra* is a downstream target of miR-731. These results suggest that exposure to OTA has a negative effect on cerebral vasculature development by interfering with the miR-731/PRLR axis in zebrafish.

1. Introduction

Ochratoxin A (OTA) is a common mycotoxin that is produced by *Penicillin* and *Aspergillu* species. Various foodstuffs such as cereal products, grapes, coffee, wine, and pork are commonly contaminated with OTA (Ostry et al., 2013). After metabolized by the liver,

* Corresponding author. Graduate Institute of Toxicology College of Medicine, National Taiwan University, No. 1,Sec 1, Jen-Ai Rd, Taipei, 10043, Taiwan.
** Corresponding author. Department of Biomedical Sciences, Chung Shan Medical University, No.110,Sec.1,Jianguo N.Rd.,Taichung City 40201,Taiwan.
E-mail addresses: fengyu@csmu.edu.tw (F.-Y. Yu), biingliu@ntu.edu.tw (B.-H. Liu).

https://doi.org/10.1016/j.chemosphere.2019.125143
0045-6535/

OTA and its derivatives can be detected in human blood serum, breast milk, and urine (Soto et al., 2016). OTA binds to albumin with high affinity leading to a long serum half-life of 35 days in humans, and it is detected in 33%–100% of samples of healthy human plasma collected in Asia and Europe (Duarte et al., 2011). OTA is also present in human umbilical cord blood serum, because of the organic anion transporter on placenta (Postupolski et al., 2006; Zimmerli and Dick, 1995). As a nephrotoxin, OTA is suspected to be one of the etiological factors that are responsible for Balkan endemic nephropathy and associated urothelial cancer (Bui-Klimke and Wu, 2015). The International Agency for Research on Cancer has classified OTA as a possible human carcinogen (group 2B) (IARC, 1993).

The teratogenic and embryotoxic capacities of OTA have been demonstrated in numerous animal models. Exposure to OTA induces neural tube defects in chicken embryos and rodent fetuses and also shows neurotoxic effects on the subventricular zone of adult mouse brain (Paradells et al., 2015; Wangikar et al., 2004a,b; Wei and Sulik, 1996). The intraperitoneal injection of OTA into pregnant mice and rats triggers brain tissue degeneration, vascular channel dilation, anencephaly, and encephalocele in fetuses (Ohta et al., 2006; Wangikar et al., 2004a,b; Ueta et al., 2010). Prenatal exposure to OTA also leads to hydrocephalus in fetal hamsters and rabbits (Hood et al., 1976; Wangikar et al., 2005). In addition, the cerebrum of OTA-fed chicks exhibits perivascular edema and massive submeningeal hemorrhage (Jameel, 2011), but the details of the mechanism remain unknown.

MicroRNA-731 (miR-731), with an ortholog of miR-425 in humans, is up-regulated upon environmental stress, including OTA exposure, in teleost fish (Schyth et al., 2015; Wu et al., 2016). The miR-731 also plays a role in arterial-venous specification (Huang et al., 2019). One of the miR-731 potential target genes is found to be *prlra* (Wu et al., 2016). In the development of vertebrates, PRLR, with prolactin and growth hormones as ligands, activates the JAKs/STAT signaling pathway and thus promotes the migration and tube formation of brain endothelial cells (Yang and Friedl, 2015). Administering OTA blocked the expression of *prlra* not only in human renal cells but also in embryonic zebrafish (Wu et al., 2016; Marin-Kuan et al., 2016).

The developmental biology of cerebral vascular formation in zebrafish and other vertebrates, including humans, proceed similarly (Fujita et al., 2011; Isogai et al., 2001; Roman et al., 2002). Therefore, embryonic zebrafish is used in the present study to examine the effects of OTA on the cerebral development and associated mechanisms. An understanding of the toxic effects of OTA on embryonic vertebrates may provide useful information for evaluating the safety of OTA and its impact on public health, especially that of pregnant women and infants.

2. Materials and methods

2.1. Test species and husbandry

Wild-type (WT) AB strain zebrafish (*Danio rerio*), transgenic line Tg(fli-1: EGFP) showing green fluorescence in blood vessels, and double transgenic line Tg(fli-1a:EGFP; gata1:DsRed) with green fluorescence in blood vessels and red fluorescence in erythrocytes were kindly provided by the Taiwan Zebrafish Core Facility at Academia Sinica (TZCAS, Taipei). All fish were raised at 28 °C with a 14 h/10 h light/dark cycle. Anesthesia and euthanasia of zebrafish was conducted according to Matthews and Varga (2012). All procedures regarding zebrafish were performed in compliance with the relevant laws and institutional guidelines, and the Institutional Animal Care and Use Committee(s) have approved the experiments (IACUC approval number: 20140416).

2.2. OTA exposure

OTA purchased from Sigma-Aldrich Co (St Louis, MO) was first dissolved in ethanol at a concentration of 10 mM, and then further diluted with 0.01 M phosphate buffered saline (PBS) to 1 mM for storage at −20 °C; the final working concentration of ethanol in 0.5 μM OTA solution was around 0.005%. Healthy and normally developing embryos were collected at 6 h post-fertilization (hpf) under stereomicroscope (Nikon SMZ 800) and then kept in 24-well plates (10 embryos per well) in 2 ml egg water (60 μg/ml Instant Ocean® sea salts) (Westerfield, 2000) until the time of exposure for further toxin treatment.

2.3. Fluorescent imaging for transgenic zebrafish embryos

For examining the structures of cerebral vessels, the embryos from Tg(fli-1: EGFP) and Tg(fli-1a:EGFP; gata1:DsRed) were treated with solvent or OTA from 6 to 72 hpf, anesthetized by 0.0168% Tricaine (ethyl 3-aminobenzoate methanesulfonate) (Sigma-Aldrich) and then mounted on 3% methylcellulose. Lateral images of Figs. 3, 6D and 8C were taken under ZEISS Axioplan fluorescent microscope equipped with FITC/rhodamine filters (Magnification 100×). The confocal images of Figs. 1D and 2A were taken with a Zeiss LSM 510 META confocal microscope with FITC/rhodamine filters (Magnification 100×).

To observe the three-dimensional optical sections of brain in Tg(fli-1: EGFP), 6-hpf embryos were treated with solvent or 0.5 μM OTA to 72 hpf before anesthetized by 0.0168% Tricaine. The images and videos shown in Fig. 2B and supplementary data were recorded by Zeiss LightSheet Z.1 microscope with 20 x/1.0 water immersion objective lens following the manufacture's protocol.

2.4. Vascular leakage assay

Embryos of Tg(fli1a:EGFP) were treated with different levels of OTA since 6 hpf. After anesthetized by 0.4% Tricaine solution, embryos at 72 hpf were injected with 1% rhodamine-labeled dextran (lysine-fixable, 10 kDa MW, Invitrogen) in 0.01 M PBS into their sinus venous by using Nanoject II injection device (Drummond Scientific, Broomall, PA). Each of the injected embryos was imaged at 15 min post-injection under Zeiss fluorescence microscope (Axioplan) with FITC and rhodamine filters (magnification 100×).

2.5. Paraffin sectioning and staining

For paraffin sectioning, zebrafish embryos were fixed overnight in cold 4% paraformaldehyde-PBS. The fixed samples were mounted in agarose, embedded in paraffin, and then sliced into paraffin section with 4-μm thickness. Head sections were dehydrated in graded ethanol, cleared in two changes of Neo-clear (Merck) and stained with hematoxylin/eosin solution before mounted with Neo-Mount (Merck). The photos were taken under Zeiss Axioplan microscope (magnification 200×).

2.6. Ventricle injection

WT embryos at 6 hpf were treated with solvent and OTA, and then chorions of 24-hpf embryos were removed for the procedure of brain ventricle injection according to Gutzman and Sive (2009). Embryos were anesthetized in 0.0168% Tricaine (Sigma Aldrich) dissolved in egg water prior to injection and imaging. The hindbrain ventricle was microinjected with 2.3 nl of 1% rhodamine-labeled dextran (lysine-fixable, 10 kDa MW, Invitrogen) in 0.01 M PBS, which then diffused through the brain cavities. After 10 min of injection, the images were taken under a Zeiss Axioplan microscope

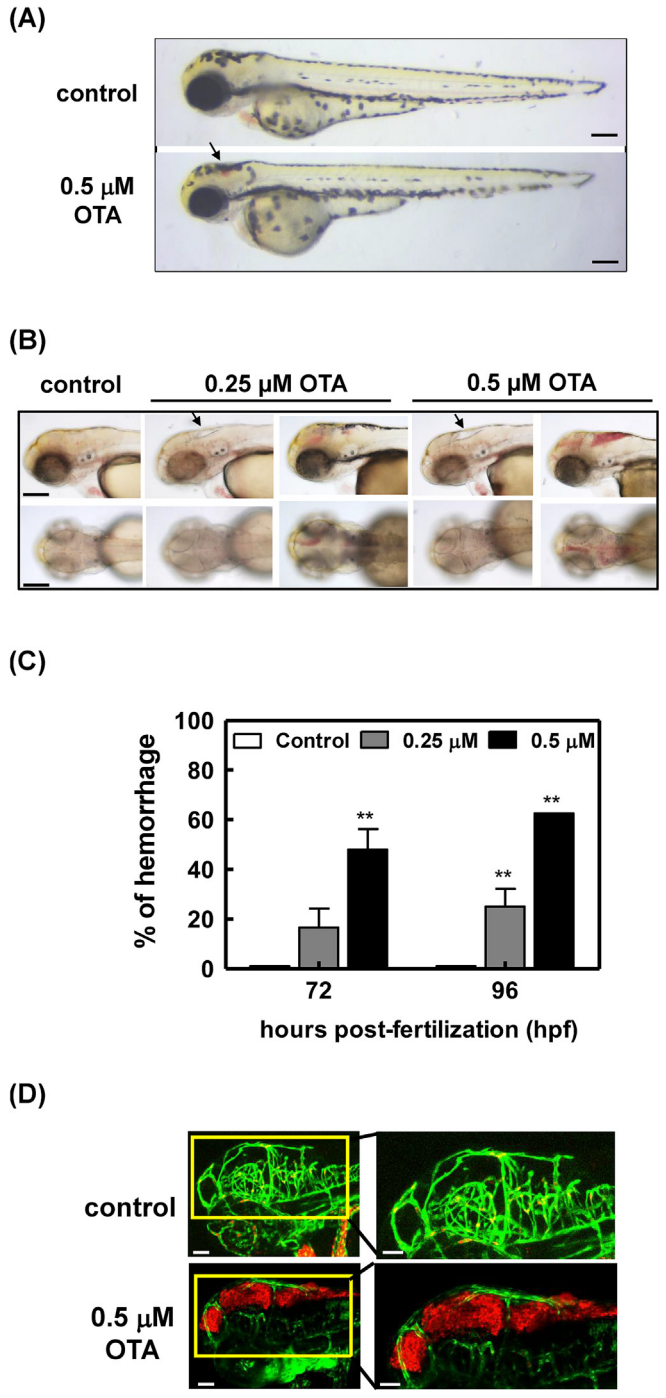

Fig. 1. OTA induced intracerebral hemorrhage in zebrafish embryos. (A) WT embryos at 6 hpf were exposed to solvent and 0.5 μM OTA. Morphology of 72 hpf embryos were obtained from the lateral view under a stereomicroscope. Scale bar, 100 μm; the arrow indicates the intracerebral hemorrhage. (B) WT embryos at 6 hpf were exposed to solvent, 0.25 and 0.5 μM OTA. The representative images of 72 hpf embryos with intracerebral hemorrhage or cavity in hindbrain areas were obtained from the lateral and dorsal views under the stereomicroscope. Scale bar, 100 μm; the arrows indicate cerebral edema. (C) The hemorrhage percentage of embryos was obtained at 72 and 96 hpf, respectively. Sixteen embryos were used in every treated group of an individual experiment. Values are represented as the mean ± SEM from 6 independent experiments. $^{**}p < 0.01$. (D) The 6 hpf embryos were obtained from Tg(fli1a:EGFP; gata1:dsRed) with blood vessels showing green fluorescence and erythrocytes showing red fluorescence, and then exposed to solvent and 0.5 μM OTA. The images of hemorrhaging head at 72 hpf were taken under the confocal microscopy. Heads to the left. Scale bar, 50 μm. (For interpretation of the references to colour in this figure legend, the reader is referred to the Web version of this article.)

(magnification 100×).

2.7. antagomiRs microinjection

The mirVana™ antagomiR-731 or mirVana™ miRNA inhibitor negative control#1 (antagomiR-NC) (Life Technologies) at a level of 1600 pg were injected into the yolk stream of 1–2 cell stage embryos by using Nanoject II injection device (Drummond Scientific, Broomall, PA). The normally developing embryos at 6 hpf were selected under steromicroscope (Nikon SMZ 800) and subsequently for solvent and OTA treatment.

2.8. mRNA levels detection

The total RNA was extracted from solvent- or OTA-treated WT embryos at 72 hpf stage and then converted with Superscript III reverse transcriptase (Invitrogen, Carlsbad, CA) to generate the complementary DNA (cDNA). PCR was conducted using cDNA as the template and designed primers as shown in Table S1 to examine the transcript levels of the following genes, including *prlra* (NM_001128677.1), *haao* (NM_001007390), *serpinc1* (NM_182863), *serpind1* (NM_182880) and *ef* (AM422110.2). The *ef* was used as an internal control.

2.9. qRT- PCR for microRNA

For miR-731 (MIMAT0003761) quantification, stem-loop reverse transcription primers designed based on Varkonyi-Gasic et al., 2007 were applied for cDNA production. The quantitative PCR was performed with specific primers (forward primer and universal-R primer), universal probeLibrary probe #21 (Roche), and FastStart Universal probe Master (Roche) (Table S1); The miR-26a was used as the reference gene. Data were obtained from ABI 7000 thermocycler and calculated according to the manufacturer's description (Thermo Fisher Scientific).

2.10. Preparation and injection of prlra cRNA

The full-length *prlra* cDNA was amplified by PCR with the following primers (*prlra* F: 5′-AGGGAATTCATGAG-GATTTCCGCCGCTG-3'; *prlra* R: 5′-GCGTCTAGAGAATTGCTTGTATA ATGGCATCAGG-3′) from a cDNA preparation of 72 hpf WT embryos. The PCR product with a size of 1818-bp fragment was cloned into pCS2+ vector. The potential pCS2+ vector harbouring *prlra* cDNA was sequenced and further linearized with Not1 restriction enzyme for cRNA generation. The capped RNA (cRNA) of *prlra* was synthesized with the mMessage mMachine kit according to the manufacturer's procedure (Ambion). The size of *prlra* cRNA was checked on agarose gel and then injected into 1–2 cell stage-Tg(fli1a:EGFP) embryos at a dose of 400 pg per embryo. The normally developing embryos at 6 hpf were selected under stereomicroscope (Nikon SMZ 800) and exposed to solvent and OTA. Living images of 72 hpf embryos were recorded under Zeiss fluorescence microscope (Axioplan). The experiment was independently repeated for four times using different batches of embryos, and at least 20 embryos were used in each treated group in every experiment.

2.11. Statistical analysis

The unpaired two-tailed Student's *t*-test was used between 2 groups. One-way ANOVA plus Tukey post hoc test was used between more than 2 groups. The statistical analyses were performed using GraphPad Prism (version 4.0, GraphPad Software Inc, San Diego, CA). All the data are presented as mean ± SEM. A p value

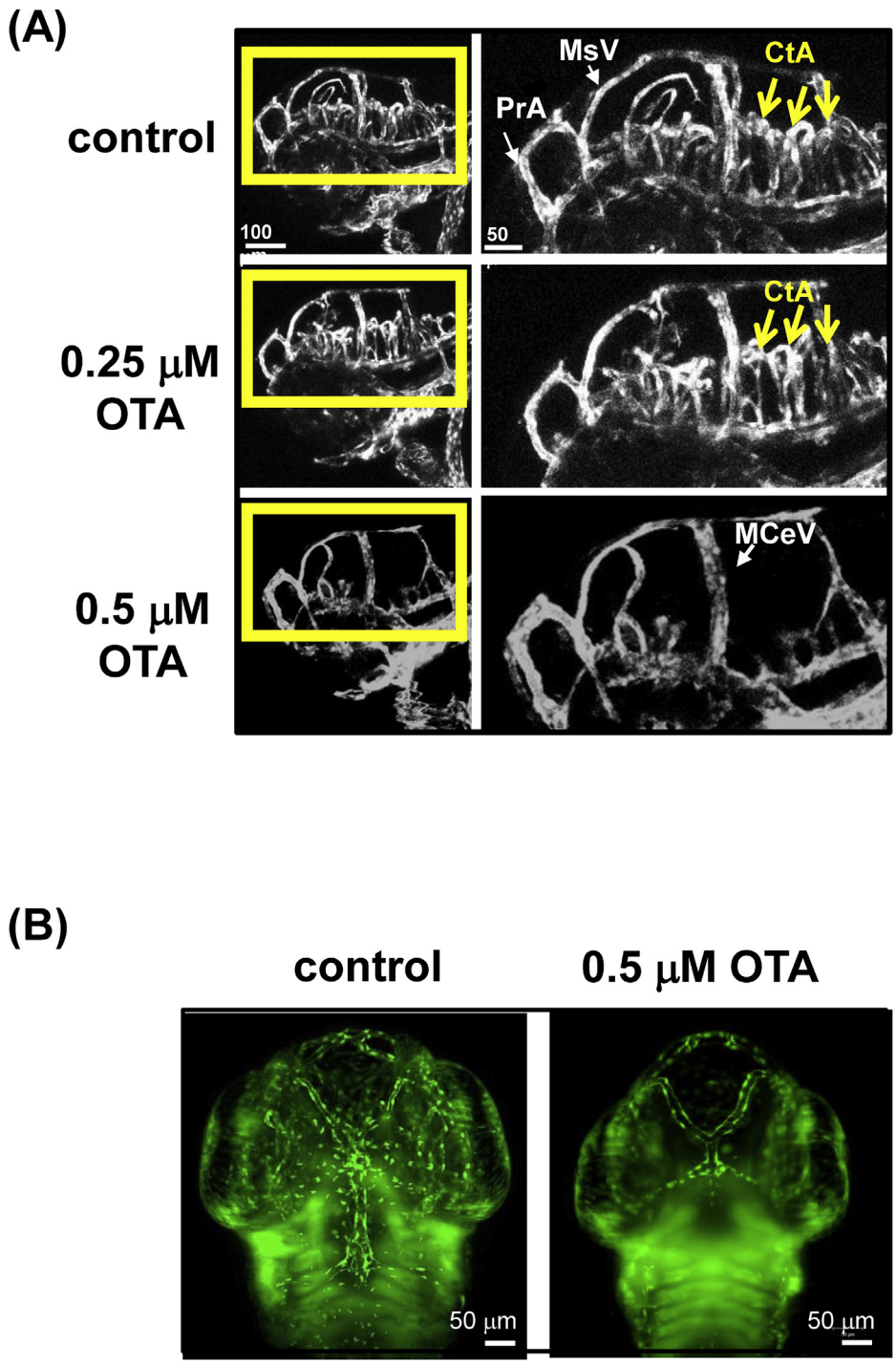

Fig. 2. OTA disrupted the vascular patterning in treated embryos. Tg(fli1a:EGFP) embryos were exposed to solvent (control) and OTA from 6 hpf till 72 hpf. Lateral confocal images (A) and dorsal lightsheet images (B) of embryonic heads were presented. PrA, prosencephalic artery; MsV, mesencephalic vein; CtA, central artery; MCeV, mid cerebral veins.

smaller than 0.05 is considered statistically significant.

3. Results

3.1. OTA induced cerebral hemorrhage in embryonic zebrafish

Zebrafish embryos at 6 hpf were exposed to solvent and OTA and then the morphology of 72-hpf embryos was presented (Fig. 1A). A hemorrhagic effect was caused by 0.5 μM OTA in the head area, but not in other body parts of embryos. Hemorrhagic sites were frequently observed in the hindbrain and occasionally in the midbrain and forebrain. The embryos without cerebral hemorrhage had a cavity-like pattern in their hindbrain ventricles, implying a possible cerebral edema (Fig. 1B).

According to Fig. 1C, the exposure of embryos to OTA significantly increased the rate of intracerebral hemorrhage in a dose-dependent manner. Around 17 and 48% of embryos at 72 hpf developed a cerebral hemorrhage after exposure to 0.25 ad 0.5 μM

OTA, respectively, and similar proportions were observed for 96-hpf embryos. The survival rate of 72-hpf embryos treated with 0.25 and 0.5 μM OTA was around 98% and 79%, respectively (Fig. S1).

When the double transgenic embryos Tg(fli1a:EGFP; gata1:DsRed) were exposed to 0.5 μM OTA, the confocal images of OTA-treated embryos revealed a massive cranial hemorrhage (Fig. 1D). Large numbers of extravasated erythrocytes with red fluorescence were detected in the forebrain, midbrain and hindbrain areas, as well as ventricular cranial interstitial spaces.

3.2. OTA altered cerebral vascular pattern in embryonic brains

The cerebral vascular patterns in the embryos of transgenic fish Tg(fli1a:EGFP) were further investigated. Confocal imaging analysis demonstrated that EGFP-labeled cerebral vessels were well organized in transgenic embryos at 72 hpf that had been exposed to solvent (Fig. 2A). However, the formation of arch-shaped CtAs was disrupted in 72-hpf siblings that had been treated with 0.5 μM OTA, whereas the prosencephalic artery (PrA), mesencephalic vein (MsV) and middle cerebral vein (MCeV) appeared to remain intact. Videos and images obtained by light-sheet microscopy, by showing the three-dimensional structure of blood vessels, also provided evidence of losing cerebral vasculature in the OTA-treated group (Fig. 2B and supplementary videos). Loss of subintestinal vein (SIV), a basket-like structure over the yolk, was also observed after OTA treatment (Fig. S2A). In contrast, exposure to OTA did not distort or impair the patterning of trunk vasculature, including dorsal longitudinal anastomotic vessel (DLAV), intersegmental vessel (ISV), dorsal aorta (DA), and caudal vein (CV) (Fig. S2B).

3.3. OTA damaged vessel integrity

To examine the vessel integrity more closely, 72-hpf Tg(fli1a:EGFP) embryos that had been treated with OTA or solvent at 6 hpf were intravascularly injected with rhodamine-dextran conjugates. Leakage of rhodamine-labeled dextran serves as a sensitive indicator of damage to the vascular wall, owing to the small size of dextran (Atkinson et al., 1991). Under a fluorescent microscope, leakage signals of red fluorescence were detected in the hindbrain region of the 0.25 μM OTA-treated group (Fig. 3). Exposure to 0.5 μM OTA caused the hindbrain segment of embryos to become fully congested with diffused rhodamine-dextran; fluorescence was also observed in the forebrain and midbrain areas. Dye leakage in periventricle and intraventricle regions indicated the impairment of blood vessel integrity by OTA.

3.4. Histology of brain sections of OTA-treated embryos

Histological sections through the hindbrain of 72-hpf WT embryos were examined. Transverse sections of fixed embryos showed that the phenotypes of solvent- and OTA-treated groups differed greatly (Fig. 4). An anomalous cavity with reduced tissue mass and defective organization was identified in the hindbrain segment of 0.5 μM OTA-exposed embryos. Erythrocyte-like cells, as indicated by the arrows, were scattered in the cavity in response to the presence of 0.5 μM OTA.

3.5. OTA impaired the early development of brain ventricles

The early stage of ventricle opening was characterized by in vivo dye labeling (Gutzman and Sive, 2009). The rhodamine-labeled dextran was injected into the 24-hpf embryo to examine the ventricle morphology. As shown in Fig. 5, the brain structure of the 24-hpf embryos that had been exposed to 0.25 and 0.5 μM OTA exhibited ventricle defects, as indicated by arrows. Lateral images showed that both midbrain and hindbrain regions in the 0.5 μM OTA-exposed group remained apposed, without full ventricle expansion. Similarly, dorsal images revealed the expansion of all ventricles was very limited in both the 0.25 and 0.5 μM OTA-treated embryos.

3.6. AntagomiR-731 reversed OTA-induced intracerebral hemorrhage

We have reported the up-regulation of miR-731 expression in OTA-treated embryos in the microRNA profiling based on RNA sequencing (Wu et al., 2016). In the present study, treatment of embryos with 0.5 μM OTA increased the miR-731 levels to 6.8 ± 1.5 folds of control in the 72-hpf embryonic fish, and the presence of antagomiR-731 significantly suppressed the levels of miR-731 induced by OTA (Fig. 6A). Fig. 6B displays representative head phenotypes of the 72-hpf embryos following solvent and OTA treatments. Administering 0.5 μM OTA to embryos that had been injected with antagomiR-NC caused 31.3 ± 5.3% of them to exhibit intracerebral hemorrhage (Fig. 6C). Injection of the antagomiR-731

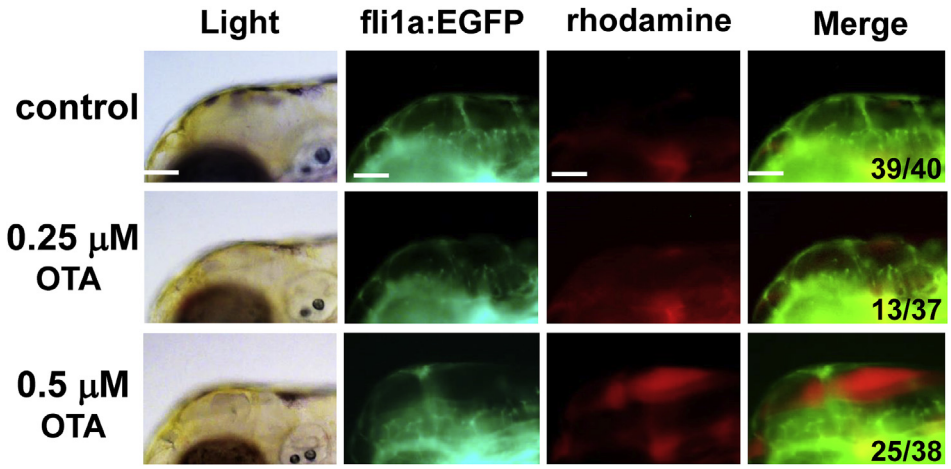

Fig. 3. OTA triggered vascular leakage of embryos. The embryos of Tg(fli1a:EGFP) were exposed to solvent (control), 0.25 and 0.5 μM OTA since 6 hpf, and then 10 kDa rhodamine-labeled dextrans were injected into sinus venous of embryos at 72 hpf. Fifteen-minute post-injection, the fluorescence of leaked dye in brain areas was recorded with a fluorescence microscope (magnification 100×). Lateral view with the head to the left. Scale bar, 100 μm.

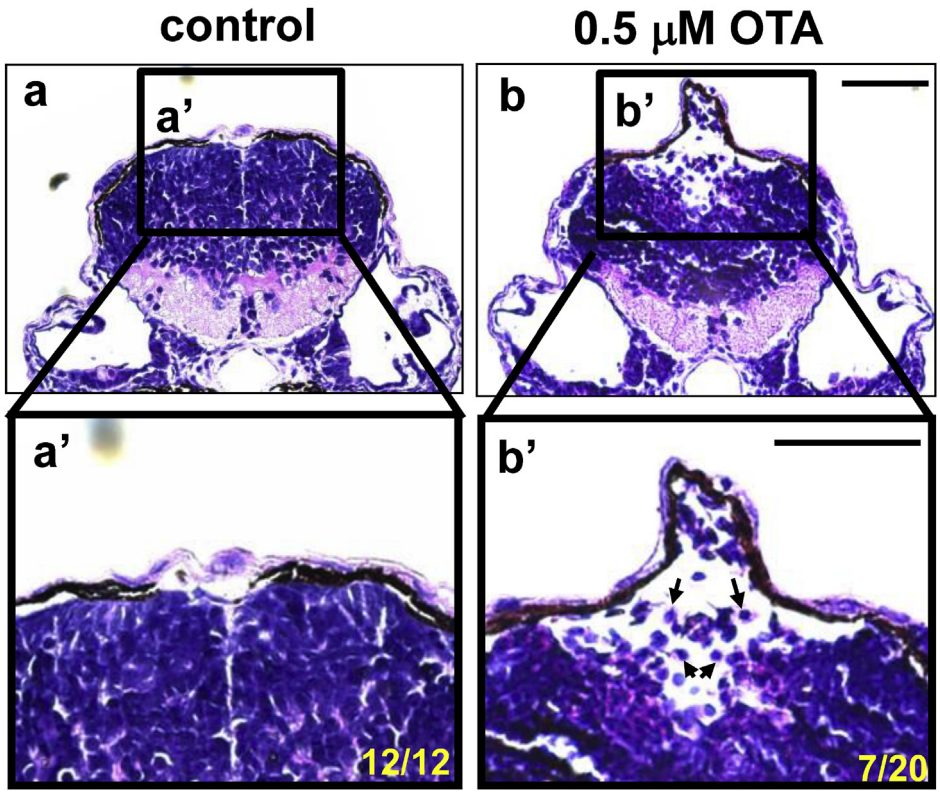

Fig. 4. OTA impaired histological structure of embryonic brain. WT embryos at 6 hpf were exposed to solvent (control) and 0.5 μM OTA. Transverse histological sections (4 μm) were obtained at 72 hpf and further stained with hematoxylin and eosin. The (a', b') derived from (a, b) are enlarged figures of hindbrain area. The arrows in b' indicate the red blood cells. Scale bar, 50 μm. (For interpretation of the references to colour in this figure legend, the reader is referred to the Web version of this article.)

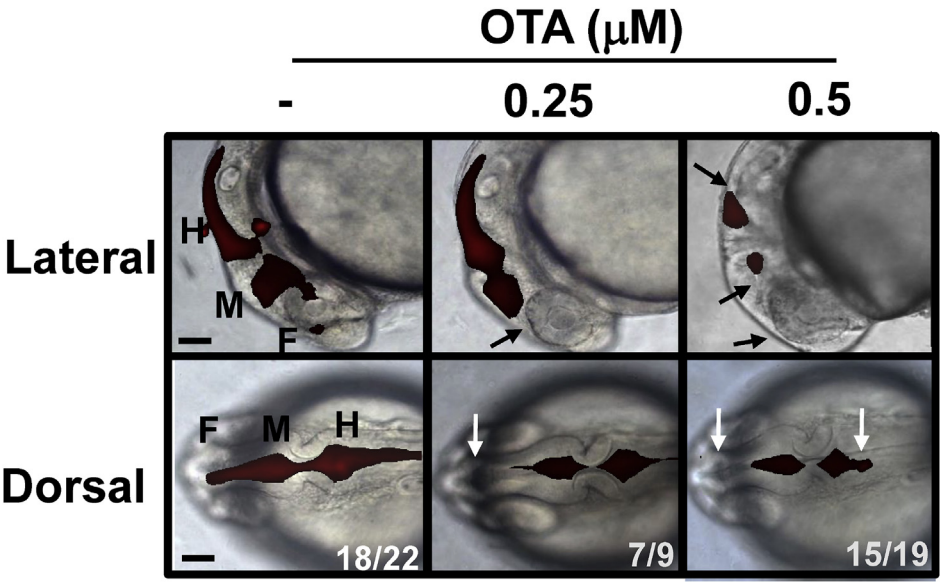

Fig. 5. The abnormal ventricle expansion in OTA-treated embryos. WT zebrafish embryos were treated with solvent, 0.25, or 0.5 μM OTA since 6 hpf. Embryos at 24 hpf were injected 10 KDa rhodamine-labeled dextrane into the hindbrain ventricles. The lateral and dorsal images were taken under the fluorescent microscope at 10 min post-injection. Arrows indicate ventricle defects. Scale bar, 100 μm; F, forebrain ventricle; M, midbrain ventricle; F, hindbrain ventricle.

significantly reduced the percentage of defective embryos to 15.4 ± 4.7% (17 out of 118). A similar protocol was applied to the embryos of Tg(fli1a:EGFP). As shown in Fig. 6D, the microinjection of antagomiR-NC caused approximately 30% of the Tg embryos (n = 15/50) to lose their intact CtA structure in 0.5 μM OTA group. However, the presence of antagomiR-731 partially reversed the adverse effect of OTA on CtAs, such that 90.9% of embryos (n = 40/44) exhibited a relatively normal vascular structure and only 9.1% of them lose CtA vessels (n = 4/44). This result suggests that miR-731 is involved in OTA induced-cerebral hemorrhage and blood vessel

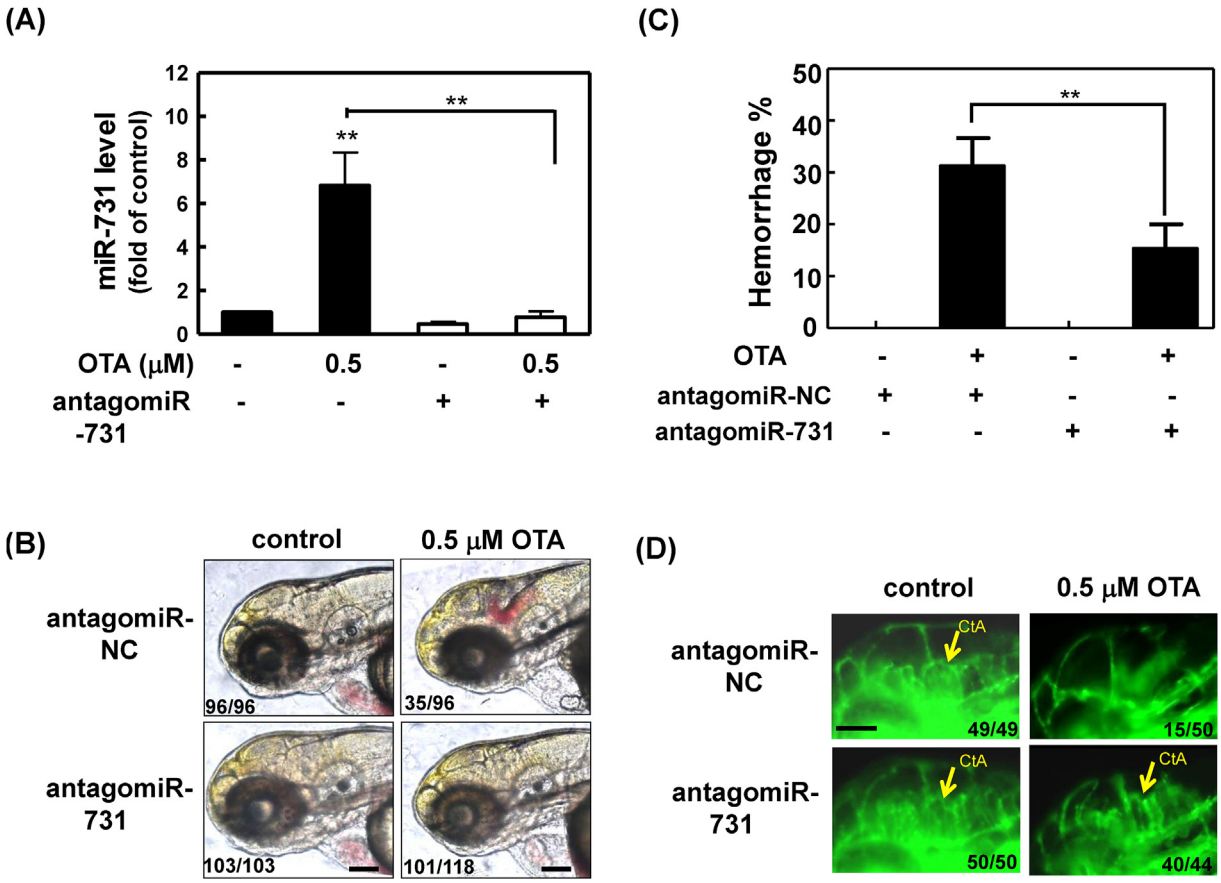

Fig. 6. The antagomiR-731 rescued the intracerebral hemorrhage caused by OTA. WT and Tg(fli1a:EGFP) embryos at 1–2 cell stage were injected with 1600 pg of antagomiR-NC (negative control) or antagomiR-731, and then treated with solvent (control) or 0.5 μM OTA at 6 hpf. (A) The miR-731 levels in solvent- and OTA-treated WT embryos were determined at 72 hpf by qRT-PCR. (B) The representative head phenotypes of WT embryos at 72 hpf under stereomicroscope. Scale bar, 100 μM. (C) The percentage of WT embryos with hemorrhagic phenotype was determined at 72 hpf by dividing the number of embryos showing intracerebral hemorrhage with the total surviving number. The data represent mean ± SEM from six independent experiments(at least 15 embryos/dose/replicate). **$p < 0.01$, significantly different between compared groups. (D) The cerebral vascular pattern in 72 hpf Tg(fli1a: EGFP) embryos from the lateral view under a fluorescence microscope (magnification 200×). CtA, central artery.

defects.

3.7. Effects of antagomiR-731 on gene expression

Four genes that were predictively associated with brain/vascular development and also differentially expressed (>2.0 folds) in the transcriptome profiling of OTA-exposed embryos (GEO number GSE71345) were identified as the potential miR-731 target genes using TargetsScanFish and miRMAP softwares (Fig. 7A) (Wu et al., 2018). The in silico prediction demonstrated that the miR-731 sequence was complementary to the 3′-UTR sequences of *prlra*, *haao*, *serpinc1*, and *serpind1* gene (Fig. S3). The Prolactin (PRL)/PRLR signaling promotes the expression of vascular endothelial growth factor (VEGF) (Goldhar et al., 2005). The *haao* gene is associated with sporadic cerebral small-vessel disease (Rutten-Jacobs and Rost, 2019). Serpinc 1 protein is a marker of disseminated intravascular coagulation, and Serpind 1 has an important role in vascular homeostasis (Liu et al., 2014; Tollefsen, 2007). In Fig. 7B, 0.5 μM OTA apparently down-regulated the mRNA signals of *prlra*, *haao*, *sepinc1,* and *sperpind1* genes in antagomiR NC-injected embryos. However, only the level of *prlra* transcript could be partially restored by the presence of antagomiR-731 in OTA-treated embryos at 48 and 72 hpf (Fig. 7B and C). This finding is consistent with our earlier finding that *prlra* mRNA is the downstream target of miR-731 in zebrafish (Wu et al., 2016).

3.8. OTA-triggered intracerebral hemorrhage was partially reversed by prlra cRNA

OTA is known to modulate the miR-731/PRLR/STAT5 axis in zebrafish embryos (Wu et al., 2016). Whether PRLR plays a role in OTA-induced intracerebral hemorrhage was further investigated. Introducing *prlra* cRNA into embryos reduced the degree of cerebral hemorrhage triggered by OTA (Fig. 8A). As shown in Fig. 8B, the presence of *prlra* cRNA significantly reduced the percentage of embryos with hemorrhage in the 0.5 μM OTA-treated group from 54.6 ± 5.3 % to 26.6 ± 7.1 %. Similarly, *prlra* cRNA restored the formation of CtA vessels in OTA-exposed groups (Fig. 8C).

4. Discussion

OTA is a widespread mycotoxin in food and feed; OTA levels in foodstuff collected from European is reported to range from 0.004 to 49.6 μM (1.4–20,000 ng/g). OTA has also been found in the ng/ml range in samples of human serum, milk, and urine (Duarte et al., 2011; Klapec et al., 2012; Soto et al., 2016). Blood samples from patients with chronic interstitial nephropathy in Tunisia have an average OTA concentration around 0.13 μM (50.4 ng/ml), with the highest level reaching 0.42 μM (171.2 ng/ml) (Hassen et al., 2004). On the other hand, the presence of 130–5420 ng/l OTA in fetal serum and cord blood samples indicates the possible exposure of human fetuses to OTA through the organic anion transporters on

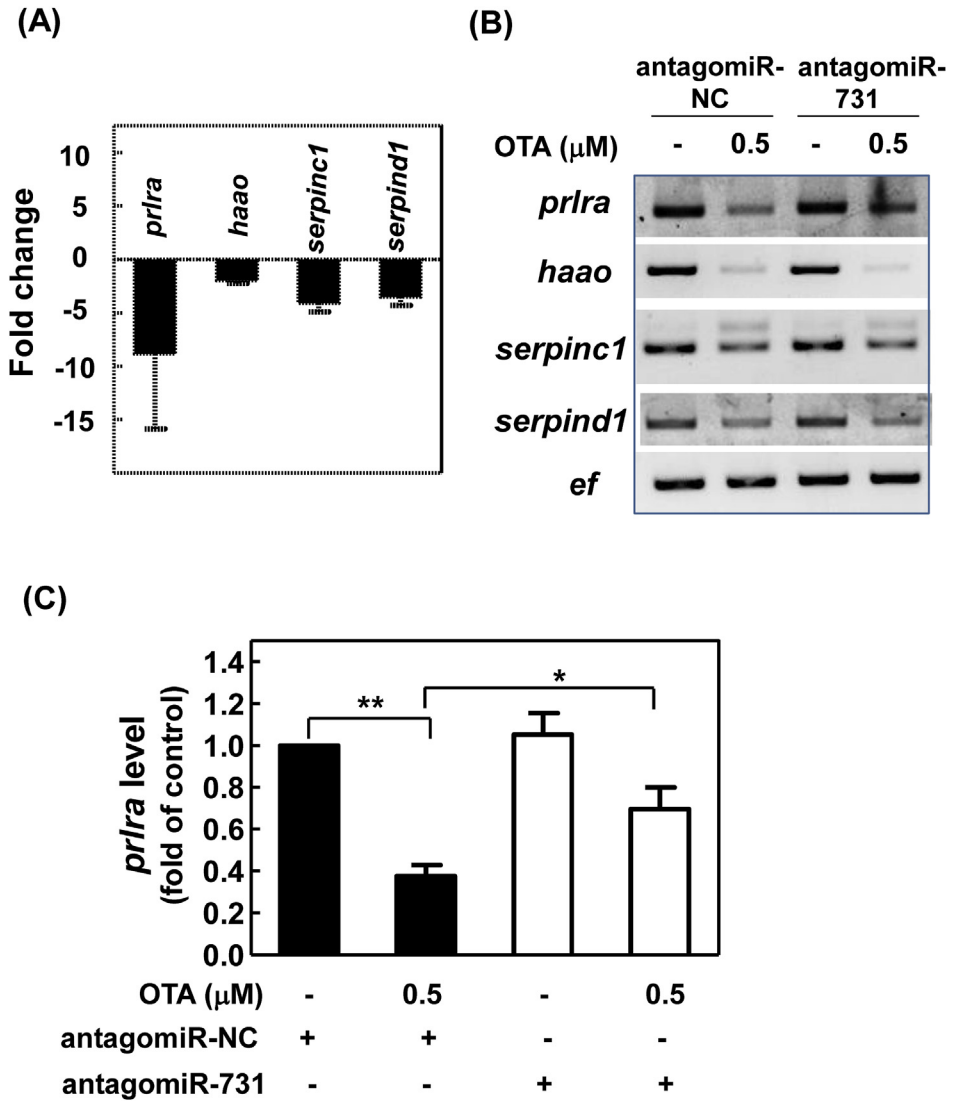

Fig. 7. Effects of OTA and antagomiR-731 on gene expression. WT embryos treated with solvent and 0.5 μM OTA were collected for microarray analysis at 48 hpf. The levels of four vascular disease-related genes, also predicted as miR-731 target genes, in microarray data (GEO umber GSE71345) were demonstrated (A). WT embryos injected with antagomiR-NC or antagomiR-731 at 1–2 cell stage were treated with solvent or 0.5 μM OTA from 6 to 48 hpf (B) and from 6 to 72 hpf (C). RT-PCR was conducted to detect the mRNA levels of *prlra*, *haao*, *serpinc 1*, and *serpind1*. The *ef* was served as an internal control. The relative levels of *prlra* in (C) were the mean ± SEM from three independent experiments (20 embryos/dose/replicate). *, $p < 0.05$; **, $p < 0.01$.

placenta (Biasucci et al., 2011; Postupolski et al., 2006; Zimmerli and Dick, 1995). The present study further demonstrated that OTA, at a detectable level in human serum, interfered with the formation of cerebral vasculature in embryonic fish, suggesting that long-term consumption of OTA-contaminated food poses a threat to early life development.

Zebrafish embryos that had been treated with 0.25 μM (100 ng/ml) and 0.5 μM (200 ng/ml) OTA suffered intracerebral hemorrhage (Fig. 1B), but no hemorrhagic phenomenon was observed in any other part of the fish (Fig. 1A). Ayed et al. (1991) reported that feeding seven day-old chicks 0.5 ng/mg OTA for four weeks leads to hemorrhage in thigh areas. Oral administration of OTA (5 mg/kg) to pregnant rats causes hemorrhaging in a significant fraction of fetuses (Malir et al., 2013). Previous studies have suggest that the hemorrhaging syndrome in rats and chickens may be attributed to defective of blood coagulation (Doerr et al., 1974; Galtier et al., 1979; Albassam et al., 1987). We have previously reported that OTA disrupts the liver development and coagulation pathway in embryonic zebrafish (Wu et al., 2018). AFB_1 is also a hepatotoxin known to suppress blood coagulation and trigger hemorrhage in the thigh/peritoneal cavity in chicks and rats (Huff et al., 1983; Witlock and Wyatt, 1978). However, it did not induce intracerebral hemorrhage in any examined embryonic zebrafish that had been exposed to the highest sub-lethal dose of AFB_1 for three days (Fig. S4A). On the other hand, OTA and citrinin (CTN) are co-occurring mycotoxins which both demonstrate renal toxicity (Vrabcheva et al., 2000). CTN-exposed zebrafish embryos develop cardiotoxicity and red blood cell accumulation in the pericardium (Wu et al., 2013), but not cerebral hemorrhaging at 72 hpf (Fig. S4B). These findings suggest that impairment of kidney, liver, or heart functions does not directly correlate with OTA-induced intracerebral hemorrhage.

The defective development of CtA after OTA exposure may result in the plasma and erythrocyte leakage from the impaired CtA structures during vascular circulation, which leads to massive intracerebral hemorrhage. Comparing to other blood vessels, the CtA formation seems to be the mostly affected by OTA. OTA at

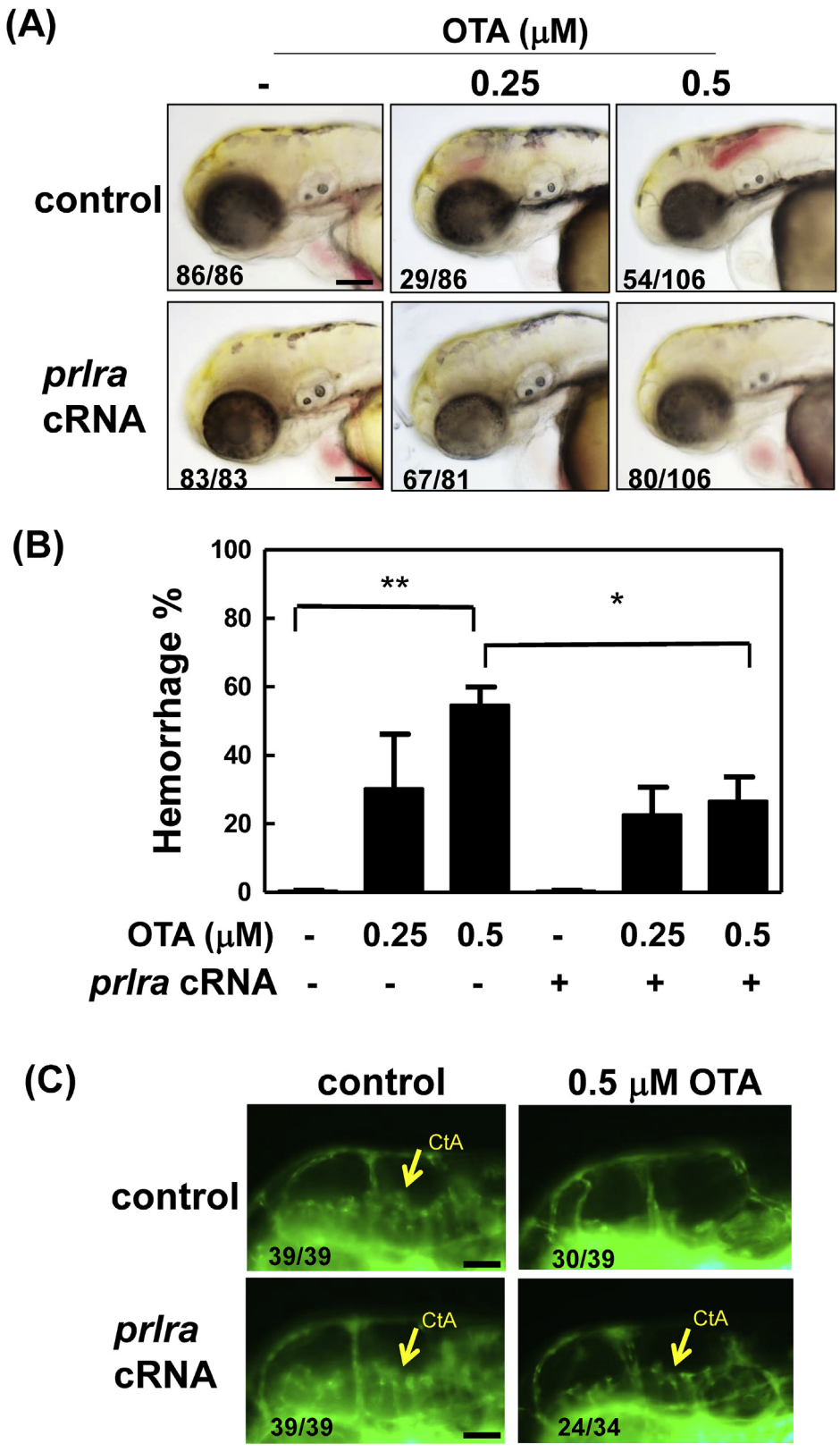

Fig. 8. The *prlra* cRNA rescued the intracerebral hemorrhage caused by OTA. Tg(fli1a:EGFP) embryos at 1–2 cell stage were injected with 400 pg of control or *prlra* cRNA, and then treated with solvent, 0.25 or 0.5 μM OTA at 6 hpf. (A) The representative head morphology of Tg(fli1a:EGFP) embryos after control and *prlra* cRNA introduction and toxin exposure. All the images were taken at 72 hpf under stereomicroscope (magnification 100×). (B) The percentage of hemorrhaging phenotype in Tg(fli1a:EFGP) embryos was determined at 72 hpf by dividing the number of embryos showing intracerebral hemorrhage with the total surviving number. The data represent mean ± SEM from four independent experiments (at least 20 embryos per dose per replicate). $^{*}p < 0.05$; $^{**}p < 0.01$. (C) The cerebral vascular pattern in Tg(fli1a:EGFP) embryos after *prlra* cRNA introduction and OTA exposure. All the images were taken at 72 hpf from the lateral view under a fluorescence microscope (magnification × 200). CtA, central artery. Scale bar, 100 μm.

0.5 μM did not apparently change the patterns of PrA/MsV/MceV in brain and those of DA/DLAV/ISV on the trunk (Fig. 2A and Fig. S2B). The selective damaging effect of OTA against cerebral vessels, especially CtAs, is unclear. CtA sprouts arise from the migration of primordial hindbrain channels (PHBC)-derived endothelial cells around 32–36 hpf and then invade the hindbrain by extending into the neural tube. OTA administration is reported to cause neural tube defects in chicken embryos and rodent foetuses (Wangikar et al., 2004a,b; Wei and Sulik, 1996). Subsequently, CtA sprouts connect with basilar artery (BA) on the midline around 40–48 hpf (Fujita et al., 2011; Ulrich et al., 2011). The network among CtA, PHBC, and BA is critical for hindbrain vascular patterning. Nevertheless, the inhibition of VEGF signalling at certain stages only seriously damages the formation of CtA instead of PHBC and BA (Ulrich et al., 2011), suggesting that locale- and stage-specific guidance factors are required for the development of various blood vessels. Comparing to cerebral vasculature, the patterning of the trunk vasculature in zebrafish is directed by a number of different cues, such as certain somite-derived molecules for regulating ISV (Torres-Vázquez et al., 2004; Fujita et al., 2011).

The antagomiR-731 protected embryos against cerebral hemorrhage induced by OTA and rescued the morphological defects of CtAs (Fig. 6). The miR-731, associating with miR-462 to form a gene cluster in fish genome, is highly expressed following hypoxic stress, viral infection, and OTA treatment (Huang et al., 2015; Zhang et al., 2016; Wu et al., 2016). Huang et al. (2019) also demonstrated that the teleost-conserved miR-462/miR-731 cluster is crucial in regulating arterial-venous specification and angiogenesis in zebrafish, which support our finding that miR-731 plays a role in embryonic vascular development. However, unlike antagomiR-731, the injection of antagomiR-462 into zebrafish embryos showed no effect on restoring the phenomena of intracerebral hemorrhage triggered by OTA (data not shown).

The *prlra* gene is known to be the downstream target of miR-

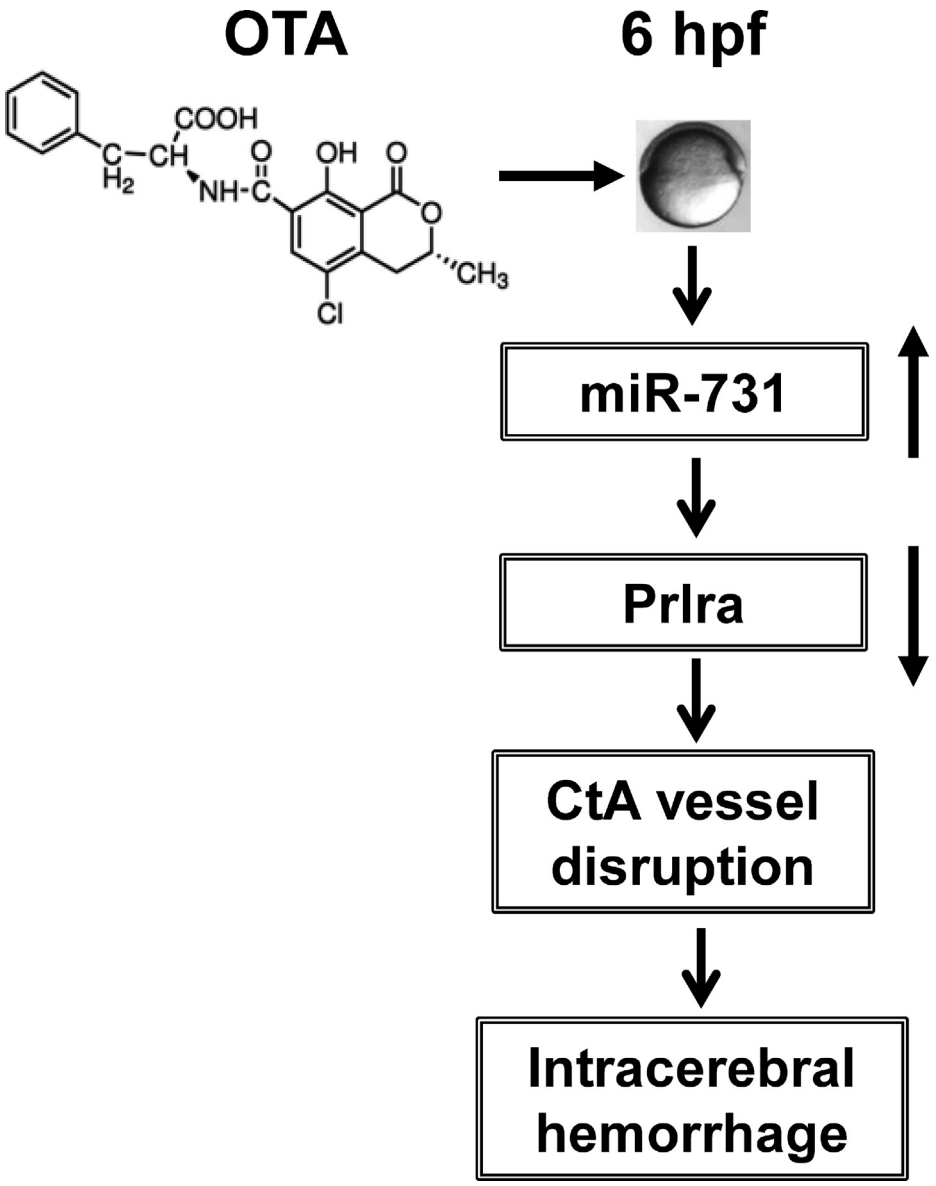

Fig. 9. A putative model depicts the mechanism of OTA-induced vascular malformation and subsequent intracerebral hemorrhage in embryonic zebrafish. Supplementary video. OTA disrupted the vascular patterning in treated embryos. Tg(fli1a:EGFP) transgenic embryos were exposed to solvent (control) and 0.5 μM OTA at 6 hpf. The images of vascular phenotype at 72 hpf were taken under a Lightsheet fluorescence microscope.

731. OTA exhibits its renal toxicity in zebrafish by upregulating miR-731 and then block the expression of *prlra* (Wu et al., 2016). PRL acts as proangiogenic factor by direct actions on endothelial cells, and PRL/PRLR transduction induces the expression of VEGF in both mouse mammary epithelial and rat lymphoma cells (Goldhar et al., 2005). Furthermore, PRL protects brain endothelial cells against methamphetamine-induced cerebral vascular toxicity by increasing the levels of tight junction proteins (Rosas-Hernandez et al., 2013), supporting our finding that PRLR signalling pathway is critical in maintaining the integrity of blood vessels.

Ligands binding to PRLR mediates several signalling cascades, including JAK2/STAT5, PI3K/AKT, Ras/MAPK, and Tek/Rac1pathways (Clevenger et al., 2003). OTA is reported to attenuate the phosphorylation of AKT and STAT5 through decreasing *prlra* expression in zebrafish (Wu et al., 2016). Decreased phospho-AKT level is observed in the rat model showing intracerebral hemorrhage (Xi et al., 2017). Besides, STAT5 phosphorylation is important in promoting angiogenesis, especially in human and mouse brain microvascular endothelial cells (Yang et al., 2013; Yang and Friedl, 2015).

5. Conclusion

OTA is detected in the blood and milk samples of pregnant women, as well as in fetal cord blood. The transplacental transfer of OTA has also been demonstrated in rats and horses, suggesting its potential threat to early life development. In the present study, we have shown that OTA triggered intracerebral hemorrhage and vascular malformation in embryonic zebrafish; the possible molecular mechanism involved in is summarized in Fig. 9**.** Through the activation of miR-731 and the subsequent attenuation of *prlra* expression, OTA exerted its adverse effects on cerebral vascular development and then led to intracerebral hemorrhage. Both miR-731 and PRLR are known to play roles in angiogenesis and vascular differentiation in mammals and teleost fish. An understanding of the toxic levels and mechanism of OTA in vertebrate embryos may provide a basis for evaluating the potential health hazards of OTA on an developing individual**.**

Declaration of competing interest

Authors declare that there are no conflicts of interest.

Acknowledgements

The authors would like to thank the Ministry of Science and Technology of the Republic of China, Taiwan , for financially supporting this research under constract No. MOST 104-2320-B-002-037-MY3. Zeiss LSM 510 META confocal microscope and Real-Time PCR machine were kindly provided by the Instrument Center of Chung Shan Medical University, which is supported by MOST (Taiwan, ROC), Ministry of Education and Chung Shan Medical University.

Appendix A. Supplementary data

Supplementary data to this article can be found online at https://doi.org/10.1016/j.chemosphere.2019.125143.

References

Albassam, M.A., Yong, S.I., Bhatnagar, R., Sharma, A.K., Prior, M.G., 1987. Histopathologic and electron microscopic studies on the acute toxicity of ochratoxin A in rats. Vet. Pathol. 24 (5), 427–435.

Atkinson, E.G., Jones, S., Ellis, B.A., Dumonde, D.C., Graham, E., 1991. Molecular size of retinal vascular leakage determined by FITC-dextran angiography in patients with posterior uveitis. Eye 5 (Pt 4), 440–446.

Ayed, I.A., Dafalla, R., Yagi, A.I., Adam, S.E., 1991. Effect on ochratoxin A on lohmann-type chicks. Vet. Hum. Toxicol. 33 (6), 557–560.

Biasucci, G., Calabrese, G., Di Giuseppe, R., Carrara, G., Colombo, F., Mandelli, B., Maj, M., Bertuzzi, T., Pietri, A., Rossi, F., 2011. The presence of ochratoxin A in cord serum and in human milk and its correspondence with maternal dietary habits. Eur. J. Nutr. 50 (3), 211–218.

Bui-Klimke, T.R., Wu, F., 2015. Ochratoxin A and human health risk: a review of the evidence. Crit. Rev. Food Sci. Nutr. 55 (13), 1860–1869.

Clevenger, C.V., Furth, P.A., Hankinson, S.E., Schuler, L.A., 2003. The role of prolactin in mammary carcinoma. Endocr. Rev. 24, 1–2.

Doerr, J.A., Huff, W.E., Tung, H.T., Wyatt, R.D., Hamilton, P.B., 1974. A survey of T-2 toxin, ochratoxin, and aflatoxin for their effects on the coagulation of blood in young broiler chickens. Poult. Sci. 53 (5), 1728–1734.

Duarte, S.C., Pena, A., Lino, C.M., 2011. Human ochratoxin a biomarkers–from exposure to effect. Crit. Rev. Toxicol. 41 (3), 187–212.

Fujita, M., Cha, Y.R., Pham, V.N., Sakurai, A., Roman, B.L., Gutkind, J.S., Weinstein, B.M., 2011. Assembly and patterning of the vascular network of the vertebrate hindbrain. Development 138 (9), 1705–1715.

Galtier, P., Boneu, B., Charpenteau, J.L., Bodin, G., Alvinerie, M., More, J., 1979. Physiopathology of haemorrhagic syndrome related to ochratoxin A intoxication in rats. Food Cosmet. Toxicol. 17 (1), 49–53.

Goldhar, A.S., Vonderhaar, B.K., Trott, J.F., Hovey, R.C., 2005. Prolactin-induced expression of vascular endothelial growth factor via Egr-1. Mol. Cell. Endocrinol. 232 (1–2), 9–19.

Gutzman, J.H., Sive, H., 2009. Zebrafish brain ventricle injection. J. Vis. Exp. (26).

Hassen, W., Abid-Essafi, S., Achour, A., Guezzah, N., Zakhama, A., Ellouz, F., Creppy, E.E., Bacha, H., et al., 2004. Karyomegaly of tubular kidney cells in human chronic interstitial nephropathy in Tunisia: respective role of Ochratoxin A and possible genetic predisposition. Hum. Exp. Toxicol. 23 (7), 339–346.

Hood, R.D., Naughton, M.J., Hayes, A.W., 1976. Prenatal effects of ochratoxin A in hamsters. Teratology 13 (1), 11–14.

Huang, C.X., Chen, N., Wu, X.J., Huang, C.H., He, Y., Tang, R., Wang, W.M., Wang, H.L., 2015. The zebrafish miR-462/miR-731 cluster is induced under hypoxic stress via hypoxia-inducible factor 1alpha and functions in cellular adaptations. FASEB J. 29 (12), 4901–4913.

Huang, C.X., Huang, Y., Duan, X.K., Zhang, M., Tu, J.P., Liu, J.X., Liu, H., Chen, T.S., Wang, W.M., Wang, H.L., 2019. Zebrafish miR-462-731 regulates hematopoietic specification and pu.1-dependent primitive myelopoiesis. Cell Death Differ. 26 (8), 1531–1544.

Huff, W.E., Doerr, J.A., Wabeck, C.J., Chaloupka, G.W., May, J.D., Merkley, J.W., 1983. Individual and combined effects of aflatoxin and ochratoxin A on bruising in broiler chickens. Poult. Sci. 62 (9), 1764–1771.

IARC, 1993. monographs on the evaluation of carcinogenic risks to humans 56, 489.

Isogai, S., Horiguchi, M., Weinstein, B.M., 2001. The vascular anatomy of the developing zebrafish: an atlas of embryonic and early larval development. Dev. Biol. 230 (2), 278–301.

Jameel, F.A., 2011. Pathological effects of ochratoxin A in brain, heart and lung of chicks. Al-Anbar J. Vet. Sci. 4 (2), 93–98.

Klapec, T., Sarkanj, B., Banjari, I., Strelec, I., 2012. Urinary ochratoxin A and ochratoxin alpha in pregnant women. Food Chem. Toxicol. 50 (12), 4487–4492.

Liu, Y., Kretz, C.A., Maeder, M.L., Richter, C.E., Tsao, P., Vo, A.H., Huarng, M.C., Rode, T., Hu, Z., Mehra, R., Olson, S.T., Joung, J.K., Shavit, J.A., 2014. Targeted mutagenesis of zebrafish antithrombin III triggers disseminated intravascular coagulation and thrombosis, revealing insight into function. Blood 124 (1), 142–150.

Malir, F., Ostry, V., Pfohl-Leszkowicz, A., Novotna, E., 2013. Ochratoxin A: developmental and reproductive toxicity-an overview. Birth Defects Res B Dev. Reprod. Toxicol. 98 (6), 493–502.

Marin-Kuan, M., Nestler, S., Verguet, C., Bezençon, C., Piguet, D., Mansourian, R., Holzwarth, J., Grigorov, M., Delatour, T., Mantle, P., Cavin, C., Schilter, B., 2016. A toxicogenomics approach to identify new plausible epigenetic mechanisms of ochratoxin a carcinogenicity in rat. Toxicol. Sci. 89 (1), 120–134.

Matthews, M., Varga, Z.M., 2012. Anesthesia and euthanasia in zebrafish. ILAR J. 53 (2), 192–204.

Ohta, K., Maekawa, M., Katagiri, R., Ueta, E., Naruse, I., 2006. Genetic susceptibility in the neural tube defects induced by ochratoxin A in the genetic arhinencephaly mouse, Pdn/Pdn. Congenital. Anom. 46 (3), 144–148.

Ostry, V., Malir, F., Ruprich, J., 2013. Producers and important dietary sources of ochratoxin A and citrinin. Toxins 5 (9), 1574–1586.

Paradells, S., Rocamonde, B., Llinares, C., Herranz-Pérez, V., Jimenez, M., Garcia-Verdugo, J.M., Zipancic, I., Soria, J.M., Garcia-Esparza, M.A., 2015. Neurotoxic effects of ochratoxin A on the subventricular zone of adult mouse brain. J. Appl. Toxicol. 35 (7), 737–751.

Postupolski, J., Karlowski, K., Kubik, P., 2006. Ochratoxin a in maternal and foetal blood and in maternal milk. Rocz. Panstw. Zakl. Hig. 57 (1), 23–30.

Roman, B.L., Pham, V.N., Lawson, N.D., Kulik, M., Childs, S., Lekven, A.C., Garrity, D.M., Moon, R.T., Fishman, M.C., Lechleider, R.J., Weinstein, B.M., 2002. Disruption of acvrl1 increases endothelial cell number in zebrafish cranial vessels. Development 129 (12), 3009–3019.

Rosas-Hernandez, H., Cuevas, E., M Lantz-M Peak, S., F Ali, S., Gonzalez, C., 2013. Prolactin protects against the methamphetamine-induced cerebral vascular toxicity. Curr. Neurovascular Res. 10 (4), 346–355.

Rutten-Jacobs, L.C.A., Rost, N.S., 2019. Emerging insights from the genetics of cerebral small-vessel disease. Ann. N. Y. Acad. Sci. https://doi.org/10.1111/nyas.13998.

Schyth, B.D., Bela-Ong, D.B., Jalali, S.A., Kristensen, L.B., Einer-Jensen, K., Pedersen, F.S., Lorenzen, N., 2015. Two virus-induced MicroRNAs known only from teleost fishes are orthologues of MicroRNAs involved in cell cycle control in humans. PLoS One 10 (7), e0132434.

Soto, J.B., Ruiz, M.J., Manyes, L., Juan-Garcia, A., 2016. Blood, breast milk and urine: potential biomarkers of exposure and estimated daily intake of ochratoxin A: a review. Food Addit. Contam. Part A Chem Anal Control Expo Risk Assess 33 (2), 313–328.

Tollefsen, D.M., 2007. Heparin cofactor II modulates the response to vascular injury. Arterioscler. Thromb. Vasc. Biol. 27 (3), 454–460.

Torres-Vázquez, J., Gitler, A.D., Fraser, S.D., Berk, J.D., Pham, V.N., Fishman, M.C., Childs, S., Epsteins, J.A., Weinstein, B.M., 2004. Semaphorin-plexin signaling guides patterning of the developing vasculature. Dev. Cell 7 (1), 117–123.

Ueta, E., Kodama, M., Sumino, Y., Kurome, M., Ohta, K., Katagiri, R., Naruse, I., 2010. Gender-dependent differences in the incidence of ochratoxin A-induced neural tube defects in the Pdn/Pdn mouse. Congenital. Anom. 50 (1), 29–39.

Ulrich, F., Ma, L.H., Baker, R.G., Torres-Vázquez, J., 2011. Neurovascular development in the embryonic zebrafish hindbrain. Dev. Biol. 357 (1), 134–151.

Varkonyi-Gasic, E., Wu, R., Wood, M., Walton, E.F., Hellens, R.P., et al., 2007. Protocol: a highly sensitive RT-PCR method for detection and quantification of microRNAs. Plant Methods 3, 12.

Vrabcheva, T., Usleber, E., Dietrich, R., Martlbauer, E., 2000. Co-occurrence of ochratoxin A and citrinin in cereals from Bulgarian villages with a history of Balkan endemic nephropathy. J. Agric. Food Chem. 48, 2483–2488.

Wangikar, P.B., Dwived, P., Sinha, N., 2004a. Effect in rats of simultaneous prenatal exposure to ochratoxin A and aflatoxin B1. I. Maternal toxicity and fetal malformations. Birth Defects Res. B 71, 343–351.

Wangikar, P.B., Dwivedi, P., Sharma, A.K., Sinha, N., 2004b. Effect in rats of simultaneous prenatal exposure to ochratoxin A and aflatoxin B1. II. Histopathological features of teratological anomalies induced in fetuses. Birth Defects Res B Dev. Reprod. Toxicol. 71 (6), 352–358.

Wangikar, P.B., Dwivedi, P., Sinha, N., Sharma, A.K., Telang, A.G., 2005. Teratogenic effects in rabbits of simultaneous exposure to ochratoxin A and aflatoxin B1 with special reference to microscopic effects. Toxicology 215 (1–2), 37–47.

Wei, X., Sulik, K.K., 1996. Pathogenesis of caudal dysgenesis/sirenomelia induced by ochratoxin A in chick embryos. Teratology 53 (6), 378–391.

Westerfield, M., 2000. The Zebrafish Book. A Guide for the Laboratory Use of Zebrafish (Danio rerio), fourth ed. Univ. of Oregon Press, Eugene.

Witlock, D.R., Wyatt, R.D., 1978. Effects of Eimeria tenella infection and dietary aflatoxin on blood coagulation of young broiler chicks. Avian Dis. 22 (3), 481–486.

Wu, T.S., Yang, J.J., Wang, Y.W., Yu, F.Y., Liu, B.H., 2016. Mycotoxin ochratoxin A disrupts renal development via a miR-731/prolactin receptor axis in zebrafish. Toxicol. Res. (Camb) 5 (2), 519–529.

Wu, T.S., Yang, J.J., Yu, F.Y., Liu, B.H., 2013. Cardiotoxicity of mycotoxin citrinin and involvement of microRNA-138 in zebrafish embryos. Toxicol. Sci. 136 (2), 402–412.

Wu, T.S., Lin, Y.T., Huang, Y.T., Cheng, Y.C., Yu, F.Y., Liu, B.H., 2018. Disruption of liver development and coagulation pathway by ochratoxin A in embryonic zebrafish. Toxicol. Appl. Pharmacol. 340, 1–8.

Xi, T., Jin, F., Zhu, Y., Wang, J., Tang, L., Wang, Y., Liebeskind, D.S., He, Z., 2017. MicroRNA-126-3p attenuates blood-brain barrier disruption, cerebral edema and neuronal injury following intracerebral hemorrhage by regulating PIK3R2 and Akt. Biochem. Biophys. Res. Commun. 494 (1–2), 144–151.

Yang, X., Meyer, K., Friedl, A., 2013. STAT5 and prolactin participate in a positive autocrine feedback loop that promotes angiogenesis. J. Biol. Chem. 288 (29), 21184–21196.

Yang, X., Friedl, A., 2015. A positive feedback loop between prolactin and STAT5 promotes angiogenesis. Adv. Exp. Med. Biol. 846, 265–280.

Zhang, B.C., Zhou, Z.J., Sun, L., 2016. pol-miR-731, a teleost miRNA upregulated by megalocytivirus, negatively regulates virus-induced type I interferon response, apoptosis, and cell cycle arrest. Sci. Rep. 6, 28354.

Zimmerli, B., Dick, R., 1995. Determination of ochratoxin A at the ppt level in human blood, serum, milk and some foodstuffs by high-performance liquid chromatography with enhanced fluorescence detection and immunoaffinity column cleanup: methodology and Swiss data. J. Chromatogr. B Biomed. Appl. 666 (1), 85–99.